Supporting Information

Unravelling the Behavior of Dion–Jacobson Layered Hybrid Perovskites in Humid Environments

Algirdas Dučinskas[1, 2], Gee Yeong Kim[2], Davide Moia[2], Alessandro Senocrate[2], Ya-Ru Wang[2], Michael A. Hope[3], Aditya Mishra[3], Dominik J. Kubicki[4], Miłosz Siczek[5], Wojciech Bury[5], Thomas Schneeberger[1], Lyndon Emsley[3], Jovana V. Milić[1*], Joachim Maier[2*], Michael Grätzel[1*]

[1] Laboratory of Photonics and Interfaces, EPFL, 1015 Lausanne, Switzerland

[2] Max Planck Institute for Solid State Research, Heisenbergstr. 1, 70569 Stuttgart, Germany

[3] Laboratory of Magnetic Resonance, EPFL, 1015 Lausanne, Switzerland

[4] Cavendish Laboratory, University of Cambridge, CB3 0HE, Cambridge, UK

[5] Faculty of Chemistry, University of Wrocław, F. Joliot-Curie 14, 50-383 Wrocław, Poland

Email Correspondence: jovana.milic@epfl.ch, jmaier@fkf.mpg.de, michael.graetzel@epfl.ch

Table of Content

S1. Materials and Methods

Perovskite thin film preparation involved a 0.4 M $(PDMA)PbI_4$ solution which was obtained by mixing PbI_2 and $(PDMA)I_2$ powders in 1:1 equivalent molar ratio with DMF:DMSO (9:1) (v:v). $(PDMA)PbI_4$ films were solution-processed by a spin-coating procedure. The perovskite solution was dropped on the glass substrate (Assitent 50), which afterwards was spun at 1000 rpm and 4000 rpm for 10 s and 20 s, respectively. Spin-coated films were annealed on a hot plate at 150 °C for 10 min. Both solution preparation and spin-coating/annealing procedures were carried out in an argon atmosphere glovebox (0.5 ppm < O_2 and 0.5 ppm < H_2O). Prior to perovskite deposition the substrates were ultrasonically cleaned with acetone and ethanol sequentially for 5 minutes. Afterwards samples were cleaned by UV-Ozone for 15 min.

Perovskite powder preparation used mechanosynthesis. In this case the reactants were ground in a ball mill (Retsch Ball Mill MM-200) using a grinding jar (10 ml) and a ball (⌀10 mm) for 30 min at 25 Hz. The molar ratio of PbI_2 and $(PDMA)I_2$ powders was 1:1 which corresponds to the stoichiometry of $(PDMA)PbI_4$ perovskites. The resulting powders were annealed at 150 °C for 30 min.

Powder X-Ray diffraction measurements were carried out using PANalytical Empyrean Series 2 instrument in Bragg-Brentano configuration with Cu Kα radiation at 40 kV voltage and 40 mA current. For the grazing incidence measurements, the X-ray incidence angle was set at 2°. In both conditions diffracted X-rays were detected using a PIXcel3d detector.

Single crystal X-Ray diffraction. Diffraction data for $PDMAPbI_4 \times 2H_2O$ (Figure S1–S5) were collected on a Rigaku Oxford Diffraction XtaLAB Synergy-R DW diffractometer equipped with a HyPix ARC 150° Hybrid Photon Counting (HPC) detector and for $(PDMA)I_2$ on a Kuma KM4 diffractometer equipped with Sapphire CCD detector at 100 K using Mo Kα (λ = 0.71073 Å). Data were processed using the *CrystAlisPro* software.[1] The structures were solved by direct methods using SHELXS[2] and refined by full-matrix least-squares methods based on F^2 using SHELXL.[3]

UV-Vis measurements were performed using a Shimadzu UV-2600 spectrophotometer. Films were placed in an air tight quartz cuvette. During in-situ measurements the cuvette temperature was set at 29 ± 1 °C. In order to monitor humidity induced changes, the cuvette was flushed with argon gas bubbled through a deionized water vial, which was kept in a bath at 22 °C. The bath temperature was controlled by a thermostat (Julabo). The flow rate of the humidified Ar gas was 200 standard cubic centimetres per minute (sccm). After the humidity equilibrium was reached (60–70%; fluctuations due to variations in cuvette temperature), the UV-Vis absorption spectrum was recorded every 90 seconds**.**

AFM measurements: surface morphology was examined by atomic force microscopy (AFM), using a Cypher instrument (Asylum Researcher) and silicon probes.

PL measurements: steady-state photoluminescence (PL) spectra of $(PDMA)PbI_4$ on glass substrates were recorded with a Fluorolog 322 spectrometer (Horiba Jobin Yvon iHr320 and a CCD) with a bandpass of 5 nm upon excitation at 350 nm (Xenon lamp) with a band pass of 2 nm.

Thermogravimetric analysis (TGA): $(PDMA)PbI_4$ powders were exposed to 70% RH atmosphere for approximately 72 hours. The hydrated powders were then transferred to a quartz crucible and loaded on the TGA balance. Hydrated powders were heated up to 150 °C with a ramp rate of 5 °C/min and then kept at 150 °C for 30 minutes. The mass of the powder was recorded every 15 seconds. The Experiment was performed in a nitrogen atmosphere.

NMR: ^1H solid-state NMR experiments were performed at 900 MHz (21.1 T) using 1.3 mm rotors at 50 kHz magic angle spinning (MAS) with a Hahn echo pulse sequence ($\pi/2$–τ–π–τ–acquire), an echo delay, τ, of a single rotor period (20 μs), and a quantitative recycle delay of 10 s. The spectra were background subtracted with the spectrum of an empty rotor acquired under the same conditions and referenced to adamantane at 1.91 ppm. Spectra were deconvoluted using the dmfit software.[1] 15 hydrated $(PDMA)PbI_4$ thin films deposited on microscope glass were scraped for the NMR sample.

XPS: The X-ray source was Al Kα (1486.6 eV) and the binding energy scale was calibrated by setting the C—C (adventitious carbon) peak to 284.8 eV.

DFT calculations were performed with the Gaussian 09 Rev. D suite of programs[4,5] on the Fidis computer cluster of EPFL. The spacer geometry optimizations were performed at the B3LYP/6-31G(d) level of theory.

S2. X-ray Crystal Structure Analysis

The single crystals of (PDMA)Pb_2I_6×$2H_2O$ were obtained by aging of the precipitate from the post-reaction mixture obtained by mixing PDMA, MAI, PbO and concentrated aqueous solutions of HI and H_3PO_2. The structure is available on the Cambridge Structural Database under CCDC number 2041350, whereas the structure of (PDMA)I_2 can be found under CCDC number 2041787.

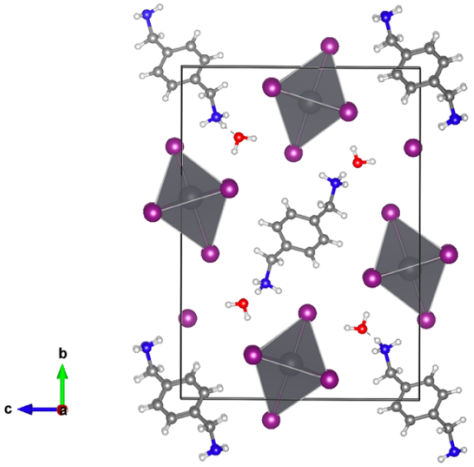

Figure S1. Crystal structure of (PDMA)Pb_2I_6×$2H_2O$ shown along the crystallographic *a*-axis.

Table S1. Selected crystal data and structure refinement parameters for (PDMA)Pb_2I_6×$2H_2O$ and (PDMA)I_2.

Chemical formula	$[C_8H_{14}N_2]Pb_2I_6$×$2H_2O$	$[C_8H_{14}N_2]I_2$
Formula Mass	1350.02	392.01
Crystal system	monoclinic	triclinic
***a* (Å)**	4.559(3)	4.534(4)
***b* (Å)**	18.958(5)	6.307(6)
***c* (Å)**	13.781(3)	10.575(9)
***α*(°)**		102.06(3)
***β* (°)**	98.94(2)	101.10(3)
***γ* (°)**		95.60(3)
***V* (Å$^{3)}$**	1176.6(9)	287.2(4)
***T* (K)**	100(2)	100(2)
Space group	*P*2_1/*n*	*P-1*
Z	2	1
Radiation type	Mo Kα	Mo Kα
No. of reflections measured	17382	2136
No. of independent reflections	3381	1114
R_{int}	0.0189	0.0673
Final R_1 values ($I > 2\sigma(I)$)	0.0133	0.0619
Final $wR(F^2)$ values ($I > 2\sigma(I)$)	0.0295	0.1580
Final R_1 values (all data)	0.0145	0.0643
Final $wR(F^2)$ values (all data)	0.0297	0.1645
Goodness of fit on F^2	1.175	1.118

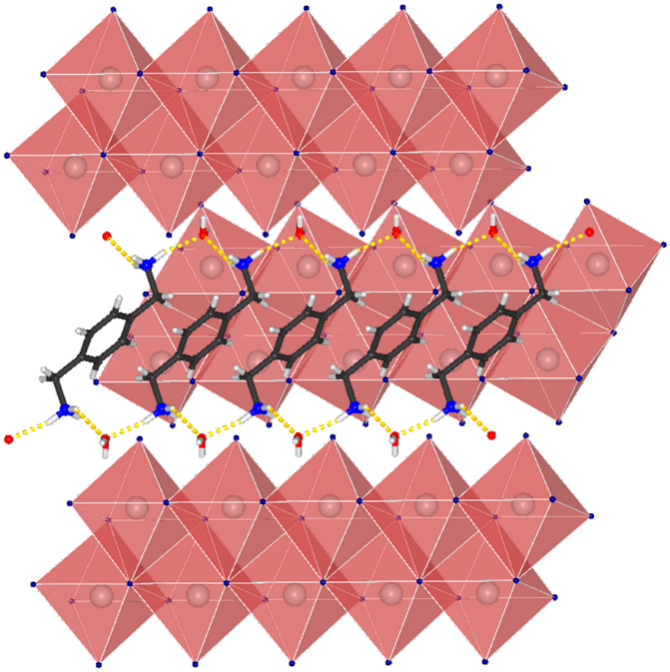

Figure S2. View of the fragment of the crystal structure of (PDMA)Pb_2I_6×2H_2O depicting the hydrogen-bonded ($PDMA^{2+}$-H_2O)$_n$ chain structure.

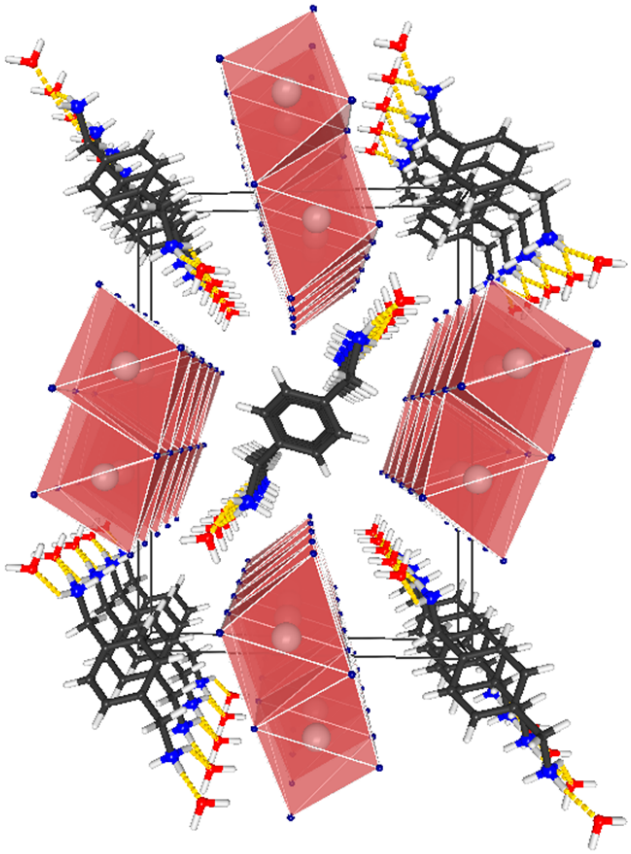

Figure S3. Perspective view of the crystal structure of (PDMA)Pb_2I_6×2H_2O shown along the crystallographic *a*-axis.

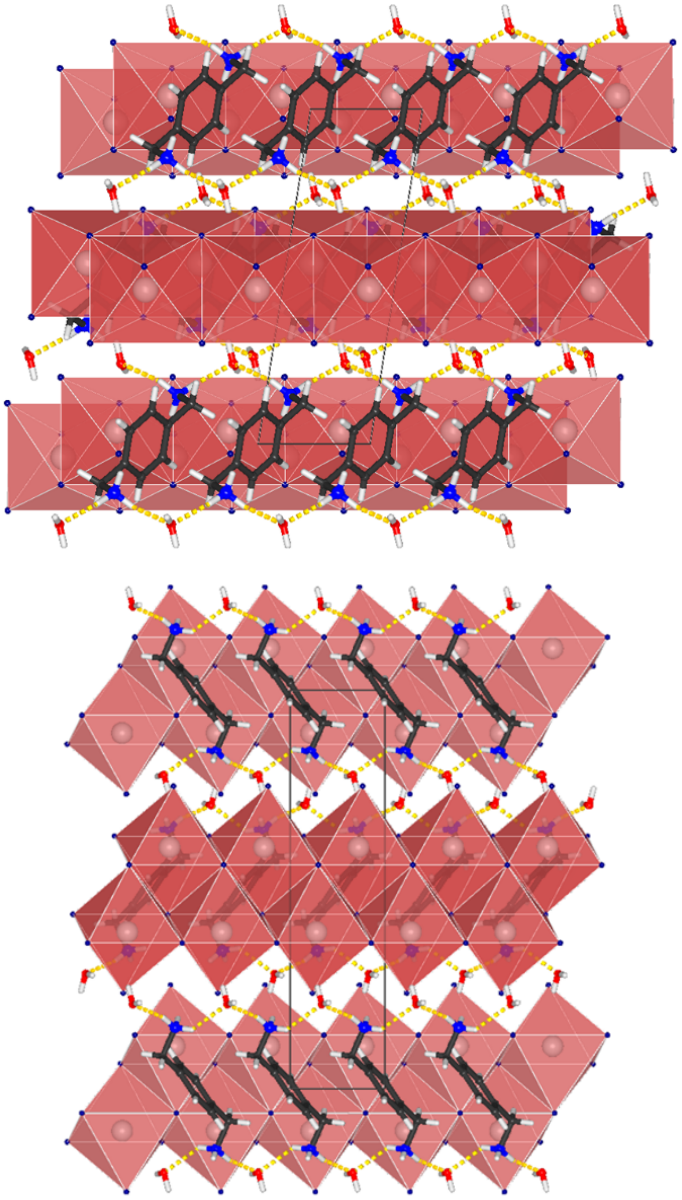

Figure S4. View of the crystal structure of (PDMA)Pb_2I_6×$2H_2O$ shown along the crystallographic *b*-axis (top) and *c*-axis (bottom).

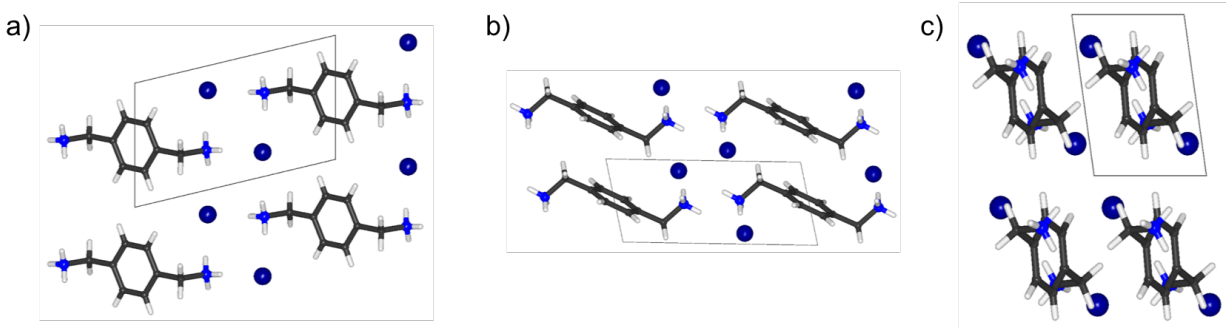

Figure S5. View of the crystal structure of (PDMA)I_2 shown along the crystallographic (a) *a*-axis, (b) *b*-axis and (c) *c*-axis.

S3. Thermogravimetric analysis of (PDMA)PbI_4 and (PDMA)I_2 powders

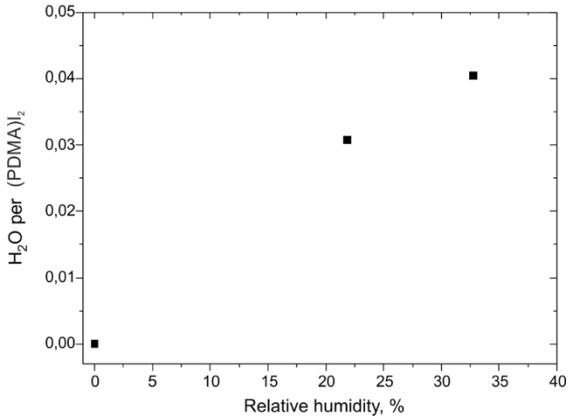

Figure S6. Hydration degree dependence of (PDMA)PbI_4 powders on the relative humidity (RH) in the range 0–37 %. Results are obtained from an in-situ hydration TGA experiment.

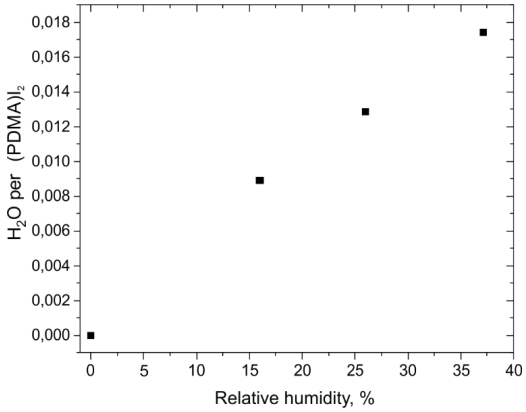

Figure S7. Hydration degree dependence of (PDMA)I_2 powders on the relative humidity (RH) in the range 0–37 %. Results are obtained from an in-situ hydration TGA experiment.

To determine the hydration degree at 70% RH, powders were hydrated ex-situ and then dehydrated during TGA measurements. The initial, anhydrous (PDMA)PbI_4 mass was 128.6 mg. After hydration and dehydration cycle the powder mass was 128.8 mg. This suggest that during the hydration and dehydration cycle only water molecules were incorporated and expelled from the powders. The in-situ recorded mass change profile with buoyancy effects included is shown in Figure S8. Considering that 2.65 ± 0.05 mg of water was taken by the powders, the ratio between water and Pb atoms is 98 ± 2 %.

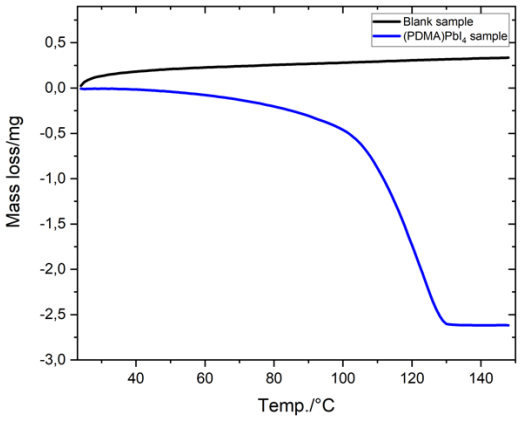

Figure S8. Mass change profile of (PDMA)PbI_4 powders that were hydrated ex-situ at 65±5 % RH for 53 hours. In order to perform the dehydration of the samples, they were heated up to 150 °C.

S4. Solid-state NMR Spectroscopy

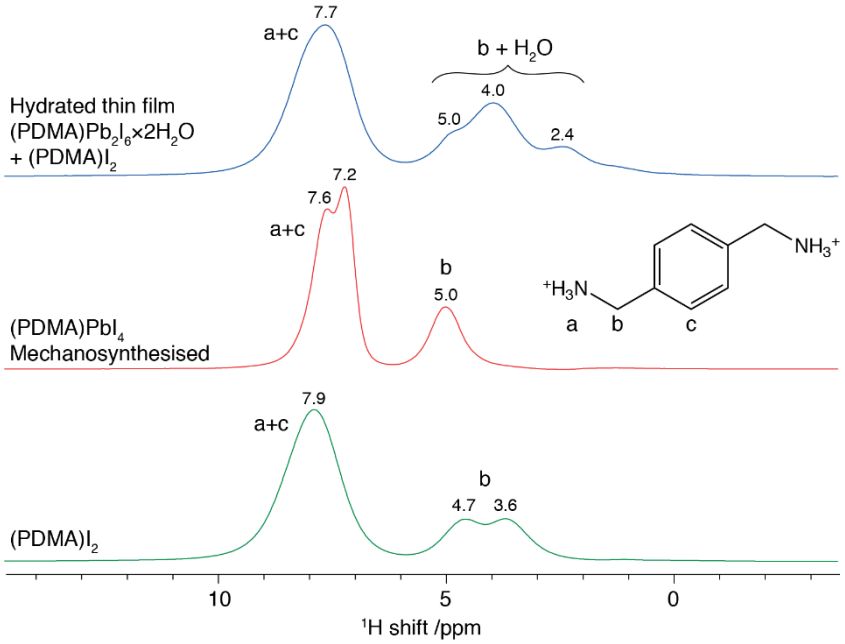

Figure S9. ^{1}H NMR spectra of $(PDMA)I_2$, mechanosynthesised $(PDMA)PbI_4$, and scraped thin films of $(PDMA)PbI_4$ following hydration. Spectra were recorded at 21.1 T and 50 kHz MAS with a Hahn echo pulse sequence and a 10 s recycle delay. Resonances are labelled with their chemical shift, and assignment according to the inset structure of $PDMA^{2+}$. Note that in $(PDMA)I_2$ there are two crystallographically distinct CH_2 (b) environments in the structure, and for the hydrated sample the $PDMA^{2+}$ resonances in $(PDMA)Pb_2I_6{\times}H_2O$ and $(PDMA)I_2$ overlap and cannot be fully resolved.

Quantification: Integrating the relative intensities of the NH_3 + aromatic (a + c) and CH_2 (b) resonances in $(PDMA)I_2$ yields a ratio of 2.67, which is in reasonable agreement with the expected ratio of 2.5 from the stoichiometry of $PDMA^{2+}$.

For the hydrated sample, it is not possible to fully resolve and assign the H_2O resonance which overlaps with the CH_2 signals from both phases. However, by taking the integration of the NH_3 + aromatic (a + c) signal, the expected integration of the CH_2 resonances can be calculated (Table S1). This integration can then be subtracted from the total integration of the CH_2 + H_2O resonances, leaving the integrated intensity for the H_2O. Comparing this intensity to the $PDMA^{2+}$ NH_3 + aromatic resonance allows the stoichiometry of hydration to be calculated, noting that a factor of 5 is needed to account for the 10 $PDMA^{2+}$ NH_3 + aromatic protons compared to two H_2O protons. If the (NH_3 + aromatic):CH_2 ratio is taken as 2.5, this yields 0.86 H_2O per $PDMA^{2+}$. If the ratio of 2.67 measured for $(PDMA)I_2$ is used, then the calculated stoichiometry is 0.99 H_2O per $PDMA^{2+}$.

Table S2. Quantification of the H_2O stoichiometry in hydrated $(PDMA)PbI_4$.

NH_3 +aromatic intensity	61.45	
CH_2 + H_2O intensity	35.17	
(NH_3 + aromatic):CH_2 ratio	2.50	2.67
CH_2 intensity	61.45 × 2.50 = 24.58	61.45 × 2.67 = 23.01
H_2O intensity	35.17 – 24.58 = 10.59	35.17 – 23.01 = 12.16
Stoichiometry	5 × 10.59 / 61.45 = 0.86	5 × 12.16 / 61.45 = 0.99

S5. Supplementary Spectral Data

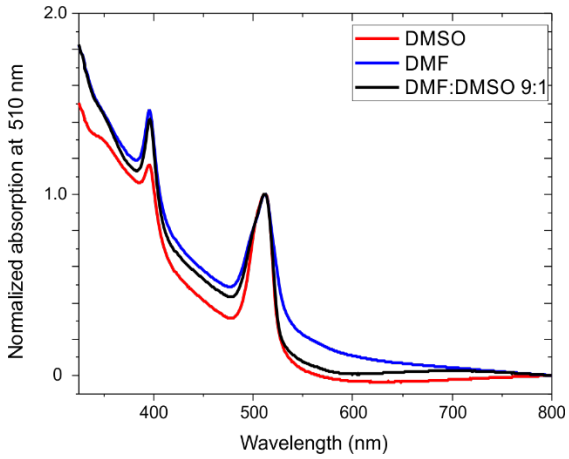

Figure S10. UV-Vis spectra of (PDMA)PbI_4 thin films that were synthesized using DMF, DMSO and DMF:DMSO 9:1 (v:v) solvents. All spectra show a resonant absorption peak located at 395 nm.

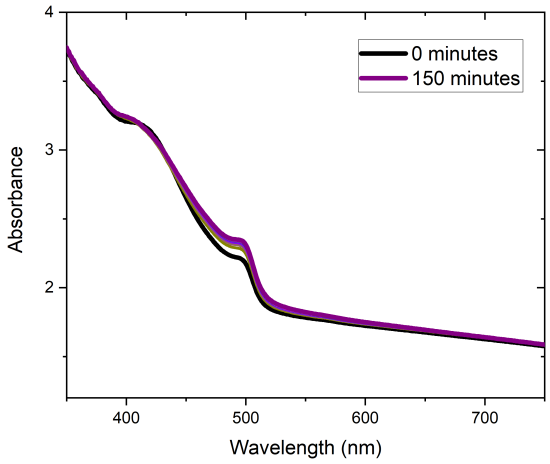

Figure S11. In-situ UV-Vis absorption spectra of a PbI_2 film during exposure to 60–70% RH. The absorption has been recorded every 90 seconds for 150 minutes.

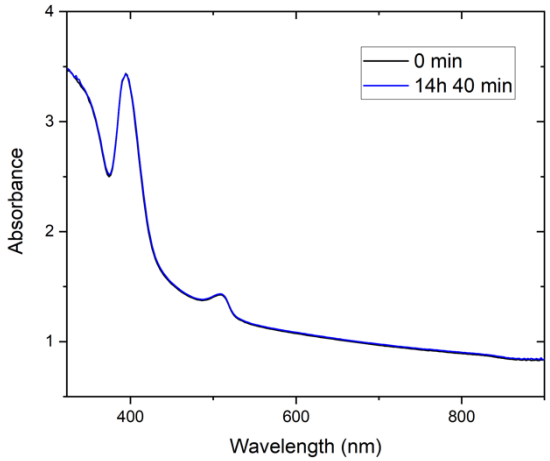

Figure S12. In-situ UV-Vis absorption of a (PDMA)PbI_4 film just after hydration (black line) and after exposure to 15% RH atmosphere for 14 h 40 min (blue line).

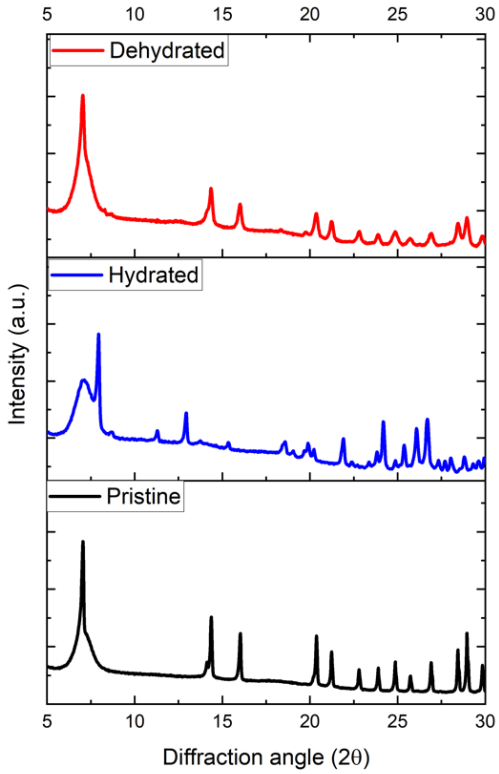

Figure S13. XRD patterns of (PDMA)PbI_4 powders in pristine (black), hydrated (blue) and dehydrated (red) condition. The dehydration was done under nitrogen atmosphere at 150 °C. The broad signal/background in the region of 7° may be due to the dome used for the in-situ measurements.

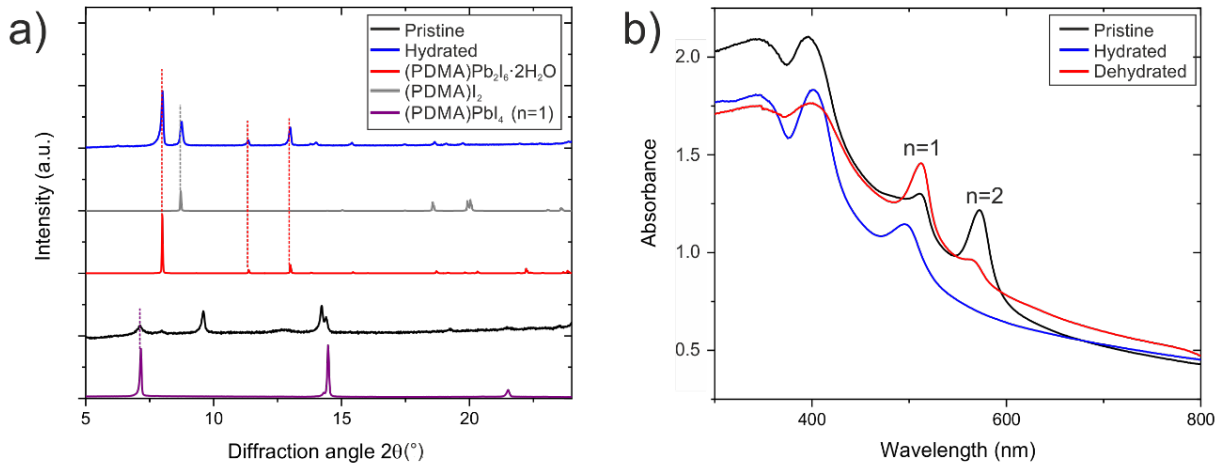

Figure S14. (a) XRD patterns of pristine (black) and hydrated (blue) (PDMA)$FAPb_2I_7$ (n = 2), pristine (purple) (PDMA)PbI_4 (n = 1) films, along with the simulated patterns of the hydrated 1D (PDMA)$Pb_2I_6{\cdot}2H_2O$ (red) and (PDMA)I_2 (grey) based on the corresponding crystal structures (Figure S1–S4). The XRD pattern of hydrated (PDMA)$FAPb_2I_7$ film show diffraction peaks that closely correspond to (PDMA)$Pb_2I_6{\cdot}2H_2O$ and (PDMA)I_2, suggesting that the hydration process of n = 2 phases is comparable to the hydration in n = 1 systems, as detailed in the main manuscript. (b) UV-Vis spectra of pristine (black), hydrated (blue), and dehydrated (red) (PDMA)$FAPb_2I_7$ n = 2 films. The excitonic peak at 571 nm is assigned to the n = 2 phase and 510 nm peak to n = 1.[7] The absorption spectrum of pristine (PDMA)$FAPb_2I_7$ films shows two distinct excitonic features, in accordance with the co-existence of the n = 1 phase,[8] which is also detected by XRD (shown in a). Upon dehydration, the n = 1 excitonic peak is enhanced, whereas n = 2 peak does not fully recover, suggesting that the system has not reverted back fully to the initial state under these conditions.

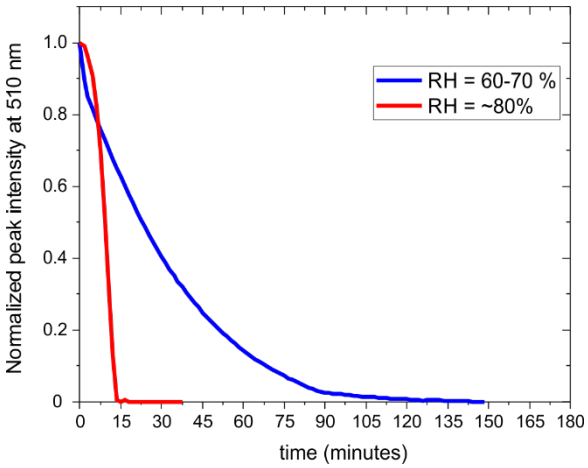

Figure S15. Time dependence of the 510 nm UV–Vis signal arising from (PDMA)PbI_4 for (PDMA)PbI_4 films at 60–70% RH (blue curve) and at ~80 % RH (red curve), showing faster hydration at 80% RH.

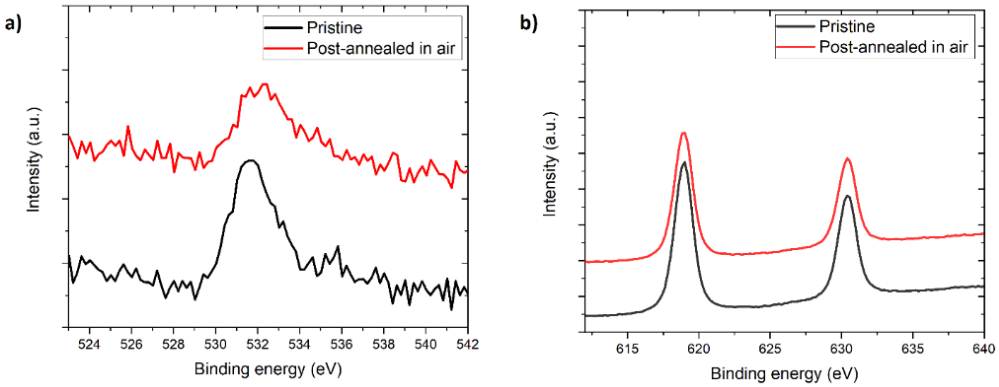

Figure S16. (a) O 1*s* XPS spectra of pristine (black) and post-annealed in air (red) samples. (b) I 3*d* XPS spectra of pristine (black) and post-annealed in air (red) samples.

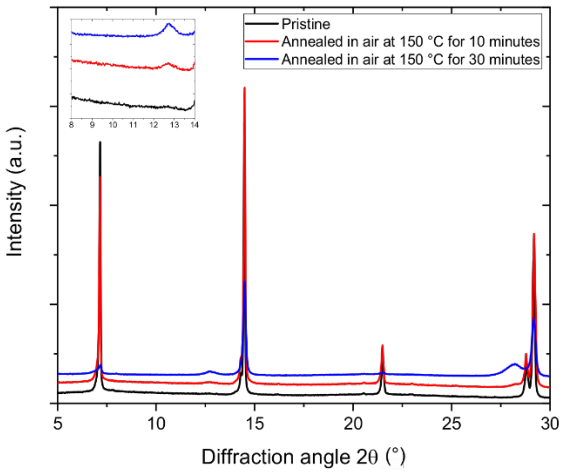

Figure S17. XRD patterns of (PDMA)PbI_4, for the pristine film (black) and for films post-annealed in air at 150 °C for 10 minutes (blue) and for 30 min (red). The inset shows the region from 8 to 14°. Here the 12.8° peak becomes more pronounced after longer annealing time, suggesting that during the air annealing process PbI_2 is gradually generated.

References

(1) CrysAlis PRO. Rigaku Oxford Diffraction: Yarnton, Oxfordshire, England, 2017.

(2) Sheldrick, G. M. A Short History of SHELX. *Acta Crystallogr*., *Sect. A: Found. Crystallogr*. **2008**, *64*, 112– 122.

(3) Sheldrick, G. M. Crystal Structure Refinement with SHELXL. *Acta Crystallogr., Sect. C: Struct. Chem.* **2015**, *71*, 3– 8.

(4) Massiot, D.; Fayon, F.; Capron, M.; King, I.; Le Calv, S.; Alonso,B.; Durand, J.-O.; Bujoli, B.; Gan, Z.; Hoatson, G. Modelling One- and Two-Dimensional Solid-State NMR Spectra. *Magn. Reson. Chem*. **2002**, *40*,70−76.

(5) *Exploring Chemistry with Electronic Structure Methods*, Second Edition. Foresman, J. B.; Frisch, A.; Gaussian, Inc.: Pittsburg, 1995.

(6) Frisch, M. J.; Trucks, G. W.; Schlegel, H. B.; Scuseria, G. E.; Robb, M. A.; Cheeseman, J. R.; Scalmani, G.; Barone, V.; Mennucci, B.; Petersson, G. A.; Nakatsuji, H.; Caricato, M.; Li, X.; Hratchian, H. P.; Izmaylov, A. F.; Bloino, J.; Zheng, G.; Sonnenberg, J. L.; Hada, M.; Ehara, M.; Toyota, K.; Fukuda, R.; Hasegawa, J.; Ishida, M.; Nakajima, T.; Honda, Y.; Kitao, O.; Nakai, H.; Vreven, T.; Montgomery Jr., J. A.; Peralta, J. E.; Ogliaro, F.; Bearpark, M.; Heyd, J. J.; Brothers, E.; Kudin, K. N.; Staroverov, V. N.; Kobayshi, R.; Normand, J.; Raghavachari, K.; Rendell, A.; Burant, J. C.; Iyengar, S. S.; Tomasi, J.; Cossi, M.; Rega, N.; Millam, J. M.; Klene, M.; Knox, J. E.; Cross, J. B.; Bakken, V.; Adamo, C.; Jaramillo, J.; Gomperts, R.; Stratmann, R. E.; Yazyev, O.; Austin, A. J.; Cammi, R.; Pomelli, C.; Ochterski, J. W.; Martin, R. L.; Morokuma, K.; Zakrzewski, V. G.; Voth, G. A.; Salvador, P.; Dannenberg, J. J.; Dapprich, S.; Daniels, A. D.; Farkas, Ö.; Foresman, J. B.; Ortiz, J. V.; Cioslowski, J.; Fox, D. J. *Gaussian 09, Revision A.1*; Gaussian, Inc.: Wallingford, CT, **2009**.

(7) Li, Y.; Milić, J. V.; Ummadisingu, A.; Seo, J.-Y.; Im, J.-H.; Kim, H.-S.; Liu, Y.; Dar, M. I.; Zakeeruddin, S. M.; Wang, P.; Hagfeldt, A.; Grätzel, M. Bifunctional Organic Spacers for Formamidinium-Based Hybrid Dion–Jacobson Two-Dimensional Perovskite Solar Cells. *Nano Lett.* **2019**, *19*, 150–157.

(8) Gélvez-Rueda, M. C.; Ahlawat, P.; Merten, L.; Jahanbakhshi, F.; Mladenović, M.; Hinderhofer, A.; Dar, M. I.; Li, Y.; Dučinskas, A.; Carlsen, B.; Tress, W.; Ummadisingu, A.; Zakeeruddin, S. M.; Schreiber, F.; Hagfeldt, A.; Rothlisberger, U.; Grozema, F. C.; Milić, J. V.; Graetzel, M. Formamidinium-Based Dion-Jacobson Layered Hybrid Perovskites: Structural Complexity and Optoelectronic Properties. *Adv. Funct. Mater.* **2020**, *30*, 2003428.